# UC Riverside
## 2018 Publications

**Title**
Potential of select intermediate-volatility organic compounds and consumer products for secondary organic aerosol and ozone formation under relevant urban conditions

**Authors**
Li, Weihua
Li, Lijie
Chen, Chia-li
et al.
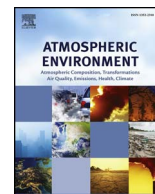
# Potential of select intermediate-volatility organic compounds and consumer products for secondary organic aerosol and ozone formation under relevant urban conditions

Weihua Li[a,b], Lijie Li[a,b,1], Chia-li Chen[a,b,2], Mary Kacarab[a,b,3], Weihan Peng[a,b], Derek Price[a,b,4], Jin Xu[c], David R. Cocker III[a,b,*]

[a] University of California, Riverside(UCR), Department of Chemical and Environmental Engineering, Riverside, CA, 92507, USA
[b] College of Engineering-Center for Environmental Research and Technology (CE-CERT), Riverside, CA, 92507, USA
[c] California Air Resources Board, Sacramento, CA, 95814, USA

## ARTICLE INFO

## ABSTRACT

Emissions of certain low vapor pressure-volatile organic compounds (LVP-VOCs) are considered exempt to volatile organic compounds (VOC) regulations due to their low evaporation rates. However, these compounds may still play a role in ambient secondary organic aerosol (SOA) and ozone formation. The LVP-VOCs selected for this work are categorized as intermediate-volatility organic compounds (IVOCs) according to their vapor pressures and molecular formulas. In this study, the evaporation rates of 14 select IVOCs are investigated with half of them losing more than 95% of their mass in less than one month. Further, SOA and ozone formation are presented from 11 select IVOCs and 5 IVOC-containing generic consumer products under atmospherically relevant conditions using varying radical sources ($NO_x$ and/or $H_2O_2$) and a surrogate reactive organic gas (ROG) mixture. Benzyl alcohol (0.41), n-heptadecane (0.38), and diethylene glycol monobutyl ether (0.16) are determined to have SOA yields greater than 0.1 in the presence of $NO_x$ and a surrogate urban hydrocarbon mixture. IVOCs also influence ozone formation from the surrogate urban mixture by impacting radical levels and $NO_x$ availability. The addition of lab created generic consumer products has a weak influence on ozone formation from the surrogate mixture but strongly affects SOA formation. The overall SOA and ozone formation of the generic consumer products could not be explained solely by the results of the pure IVOC experiments.

## 1. Introduction

Atmospheric fine particulate matter is considered to have significant effects on the earth's energy budget, human health, and visibility (Yee et al., 2013; Naeher et al., 2007; Qin et al., 2013). Secondary organic aerosol (SOA) is estimated to account for a dominant fraction of the fine particle mass in the troposphere (Hallquist et al., 2009; Cappa et al., 2016; Jathar et al., 2017; Ma et al., 2017). However, current models still cannot explain a significant portion of ambient SOA (Presto et al., 2009). In addition, emissions of volatile organic compounds (VOCs) into the air contribute to tropospheric ozone formation, higher concentration of which is a threat to human health and plant ecosystems (Finlayson-Pitts and Pitts, Jr., 1993).

The California Air Resources Board (CARB) defines a low vapor pressure-volatile organic compound (LVP-VOC) as a chemical "compound" containing at least one carbon atom with vapor pressure less than 0.1 mm Hg at 20 °C, or having more than 12 carbon atoms, or having a boiling point greater than 216 °C, or as a chemical mixture being comprised solely of compounds with more than 12 carbon atoms, or as the weight percent of a chemical mixture that boils above 216 °C (CARB, 2015). The CARB estimates LVP-VOC usage in California to be 290 tons/day (Cocker et al., 2014). These low-volatility organic compounds are widely used to produce industrial solvents, coatings, cosmetic, perfume, and pharmaceutical products (Bernard et al., 2013; Vo and Morris, 2014). Vo and Morris (2014) demonstrate that some LVP solvents being categorized as meeting the LVP-VOC nonvolatile

standards clearly volatilize at ambient conditions, nearly as rapidly as the traditional high volatility solvents they are meant to replace. Shin et al. (2016) develop and evaluate environmental modeling tools and find that when the LVP-VOC in a consumer product is volatilized from the surface to which it has been applied, greater than 90% is available for photochemical reactions either at the source location or in the downwind areas.

Select LVP-VOCs are considered as intermediate-volatility organic compounds (IVOCs) according to their vapor pressures and molecular formulas. These IVOCs have saturation concentrations ranging from 300 to $3 \times 10^6 \, \mu g \, m^{-3}$ ($1–1000 \, mg \, m^{-3}$) and are found almost entirely in the vapor phase (Donahue et al., 2012). Much heavier and less volatile IVOCs can potentially form SOA more efficiently than the more abundant but much more volatile traditional VOC SOA precursors (Robinson et al., 2007; Chan et al., 2009). Therefore, conducting research on SOA forming potential from these IVOCs helps to explain the gap between SOA model prediction and ambient measurement. However, not very much experimental work has been published on SOA formation from IVOCs. Most of the work has focused on the SOA forming potential of alkanes (straight chain, branched, and cyclic), naphthalene, alkylnaphthalenes, and exhaust from gasoline and diesel powered vehicles (as summarized below).

Several smog chamber experiments under both high and low $NO_x$ conditions confirm that SOA generated from photo-oxidation of IVOCs may be an important contributor to urban organic aerosol (OA) and should be included in SOA models (Presto et al., 2009; Tkacik et al., 2012). Gentner et al. (2012) find that on-road diesel vehicles are a major source of IVOC emissions in the Los Angeles area. Additionally, substantial formation of SOA is observed from the oxidation of diesel emissions (Weitkamp et al., 2007; Sage et al., 2008; Gentner et al., 2012). Recently, Zhao et al. (2014) estimate that primary IVOCs produce about 30% of newly formed SOA in the afternoon during the California at the Nexus of Air Quality and Climate Change (CalNex) study, about 5 times more than that from single-ring aromatics.

High SOA yields are also observed from reactions of $C_{12}$-$C_{17}$ n-alkanes, $C_{10}$-$C_{15}$ cyclic alkanes, and $C_{16}$ branched alkanes with OH radicals in the presence of high $NO_x$ in an environmental smog chamber (Lim and Ziemann, 2005, 2009; Presto et al., 2010; Loza et al., 2014). The yields from photo-oxidation of $C_{12}$ cyclic alkanes are also high under low $NO_x$ condition (Loza et al., 2014). However, Tkacik et al. (2012) do not report high yields for high-$NO_x$ photo-oxidation of $C_{12}$ straight chain, branched, and cyclic alkanes at lower $C_{OA}$ (organic aerosol concentration) that are more representative of typical atmospheric aerosol concentrations. Under low $NO_x$ conditions, the yields are high for photo-oxidation of naphthalene, 1-methylnaphthalene, and 2-methylnaphthalene (Chan et al., 2009; Chen, et al., 2016).

This work experimentally examines SOA and ozone formation from the photo-oxidation of select IVOCs and generic consumer products containing one of the select IVOCs under urban low $NO_x$ (18.7–36.4 ppb) concentrations in the presence of a surrogate mixture used to control the chamber reactivity and mimic urban atmospheric activity. Controlling chamber reactivity with a surrogate reactive organic gas (ROG) mixture has been previously explored to study ozone formation by measuring incremental reactivities of representative volatile organic compounds (VOCs) (Carter et al., 1995, 2005). The atmospheric availability of select IVOCs, SOA mass yields, ozone formation, and bulk SOA chemical composition and physical properties from select IVOCs and mixtures containing some of them are explored. This paper provides fundamentals for constraining modeling research to better estimate SOA and ozone formation from IVOCs.

## 2. Materials and methods

### 2.1. IVOC volatilization rates

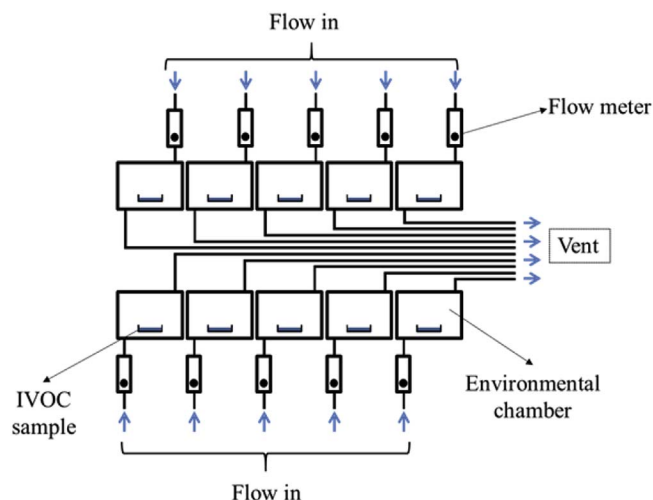Evaporation rates of individual IVOCs were studied gravimetrically



**Fig. 1.** Schematic for IVOC volatilization measurement.

within miniature ($\sim$30 L) evaporation chambers operating as continuous stirred tank reactors (CSTRs, Fig. 1). The residence time of the chambers was set to 3.5 exchanges of air per hour. The air entering these chambers was purified (Aadco 737) and had no detectable particles ($< 0.2$ particles cm-3), non-methane hydrocarbons ($< 1$ ppb), and $NO_x$ ($< 10$ ppt). The dew point of the air was less than $-60 \, °C$. The temperature of individual environmental chambers was maintained at 25° C.

The evaporative mass flux was measured by a mass balance approach with the pure compounds being placed on aluminum boats (capacity 20 ml, top I.D. 43 mm, Sigma-Aldrich) and weighed. Samples were weighed daily for the first ten days and then weekly thereafter for compounds with slow evaporative rates for a period of six months. A bank of 10 of these systems was utilized in parallel to simultaneously measure the evaporation rate of the ten IVOC samples.

### 2.2. Surrogate ROG mixture

A surrogate ROG mixture was developed by Carter et al. (1995). to represent the major classes of hydrocarbons and aldehydes measured in ambient urban atmospheres, with one compound used to represent each model species used in condensed lumped-molecule mechanism. Total surrogate concentrations used were 1.1 ppmC. The concentration of each species in the surrogate ROG mixture can be found in Table 1.

### 2.3. Photo-oxidation experiments in UCR CE-CERT environmental smog chamber

SOA and ozone formation from photo-oxidation of IVOCs were studied in the UCR CE-CERT dual indoor smog chambers (2 mil FEP Teflon film), which are described in detail elsewhere (Cocker, D. R., et al., 2001). The chambers were located in a temperature and

**Table 1**
Composition of surrogate ROG mixture.

| ppb/ppmC | Compound[a] |
|---|---|
| 20.6 | *m*-Xylene |
| 89.8 | n-Butane |
| 20.7 | n-Octane |
| 13.6 | trans-2-Butene |
| 23.1 | Toluene |
| 16.3 | Ethylene |
| 13.6 | Propylene |

[a] All the chemicals are purchased from Sigma-Aldrich ($\geq$95.0–99.0%).

humidity-controlled (< 0.1%) enclosure. Before conducting each experiment, the chambers were cleaned by reducing the chamber volume to less than 5% of its original volume while flushing the chamber with 500 L/min of purified air to make sure that the chambers had no detectable nonmethane hydrocarbons (1 ppbC detection limit), $NO_x$ (< 10 ppt), and particles (< 0.2 particles/cm$^3$). The chambers were then filled to capacity with purified air.

Known volumes of NO (Matheson, UHP grade) and $NO_2$ (generated in-situ by chemical conversion of NO) were introduced into calibrated bulbs based on calculated partial pressures and then flushed into the chambers by using 50 °C pure $N_2$ as the carrier gas. Gas phase surrogate was injected directly into the chambers at a flow rate of 0.5 LPM. Liquid phase surrogate and tracer (perfluorohexane (Sigma-Aldrich, 99%)) were injected into a small glass tube using a microliter syringe and then were vaporized in a 50 °C pure $N_2$ stream. The additional OH radical was generated via photolysis of hydrogen peroxide (SigmaAldrich, 50 wt. % in $H_2O$) which was gently heated (55–60 °C) in a small oven through glass wool (tube) and evaporated into a nitrogen stream (~5 LPM) to the chambers for about 20 min to insure an initial mixing ratio of approximately 1 ppm. The two chambers were subsequently mixed to reach identical concentrations on both sides. The two reactors were then isolated from each other and the SOA forming IVOC precursor of interest was injected into one of the chambers. The other chamber was used as control. 272 UV black lights (115 W Sylvania 350BL, $NO_2$ photolysis rate 0.4 min$^{-1}$) were turned on to initiate photo-oxidation. All experiments were conducted at 300 K in the absence of seed.

Initial precursor concentrations of IVOC (40–160 ppb, Sigma-Aldrich (≥ 95.0–99.0%)) were selected based on preliminary SAPRC-11 ozone modeling (lumped gas-phase kinetic model, see Carter et al., 2012) to ensure that a measurable and kinetically comparable change in ozone formation would be observed compared to the surrogate only case. Table S1 lists all of the experiments conducted for this study. Table 2 lists the experimental types.

### 2.4. Instrumentation

Decay of IVOCs was monitored using dual Agilent 6890 (Palo Alto, CA) gas chromatographs equipped with flame ionization detectors (GC-FID) and a Syft Technologies Voice200 Selected Ion Flow Tube-Mass Spectrometer (SIFT-MS). Ozone concentration was monitored by a Dasibi Environmental Corp. Model 1003-AH $O_3$ analyzer. A Thermo Environmental Instruments Model 42C chemiluminescence $NO_x$ analyzer was used to evaluate concentrations of NO, $NO_2$ and $NO_x$.

Particle concentrations inside the chambers were monitored using a pair of scanning mobility particle sizers (SMPS). Particle wall loss was corrected using the method described in Cocker et al. (2001). A house-built volatility tandem differential mobility analyzer (VTDMA) equipped with a Dekati thermodenuder (CSi32) was used to track the evolving volatility of SOA produced within the reaction chamber (residence time = 17 s; temperature 100°C) (Rader and McMurry, 1986; Cocker et al., 2001). Particle density was measured by a Kanomax aerosol particle mass analyzer (APM) coupled to a house-built SMPS

(Malloy et al., 2009).

The nonrefractory submicrometer particle mass and composition were monitored by an Aerodyne high-resolution time-of-flight aerosol mass spectrometer (HR-ToF-AMS) (DeCarlo et al., 2006). The HR-ToF-AMS was alternatively operated in V− and W-modes to provide both high sensitivity and high mass resolution data. AMS data were analyzed using the standard AMS data analysis software SQUIRREL v1.57 and PIKA v1.16, the standard ToF-AMS analysis toolkits written in Igor Pro 6.30 (WaveMetrics Inc., Lake Oswego, OR).

Work by the Ziemann group (Matsunaga and Ziemann, 2010) has more recently challenged the conventional assumption that the highly hydrophobic Teflon surfaces used for chamber wall material do not participate in the gas-particle equilibrium achieved within the reaction mixture inside the chamber. Matsunaga and Ziemann (2010) point out those sufficiently low vapor pressure products could participate in an equilibrium process with the wall, providing a sink for VOCs during the initial part of the experiment and a possible source later in the experiment. More recently, papers by Yeh and Ziemann (2014), Krechmer et al. (2016), Ye et al. (2016), and Zhang et al. (2014) have provided additional insight into the potential effects of chamber walls with their impacts ranging from very significant to minor. Considering direct loss of vapors to the chamber walls would likely result in higher SOA mass yields. However, these losses are uncertain and have not been accounted for by most of current smog chamber studies. Therefore, we do not make any corrections for direct loss of vapors to the chamber walls.
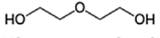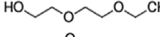
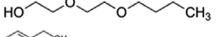### 2.5. Selection of individual IVOCs and mixtures
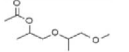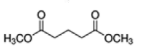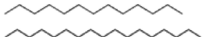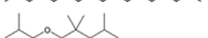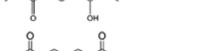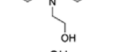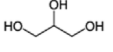
The selection of individual IVOCs and consumer products mixtures was made in direct consultation with CARB staff and the advisory committee (industry experts) set-up by CARB based on use and chemical classes. Fourteen LVP-VOCs were initially selected for analysis (Table 3); however as three (glycerol, methyl palmitate, and triethanolamine) do not evaporate significantly (< 5%) under ambient conditions over a six-month time period they were not studied as part of the subsequent environmental chamber work. Additionally, five IVOC containing consumer products were selected (recipes shown in Table S2). These generic consumer products were formulated with guidance from the Consumer Specialty Products Association (CSPA).

## 3. Results and discussion

### 3.1. Atmospheric availability of the select IVOCs

Table 3 lists chemical and physical properties of individual compounds investigated as part of this work. Oxidation state of carbon ($\overline{OS}c$) for each select chemical compound is calculated as $\overline{OS}c = 2O:C - HC$ (Kroll et al., 2011). Fig. 2 shows a 2-D space with the volatility (saturation concentration C*, μg m$^{-3}$) as the x-axis and the extent of oxidation of the select IVOCs (oxidation state of carbon) as the y-axis (Donahue et al., 2012). C* determines the amount of organic aerosol. The volatility ranges are identified with colored bands. In the

**Table 2**
Experimental conditions for SOA formation from select individual IVOCs.

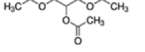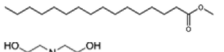| Experimental conditions | Description |
|---|---|
| IVOC + $H_2O_2$ + UV | Simplest oxidation experiment to study SOA formation from IVOC, no surrogate added. The photolysis of $H_2O_2$ increases both OH and $HO_2$ radical concentrations. |
| IVOC + NO + UV | Photo-oxidation system with individual IVOC to study directly IVOC oxidation and SOA formation. |
| Surrogate + $NO_x$ + UV | Performed in parallel as control for surrogate containing experiments described immediately below. |
| IVOC + Surrogate + $NO_x$ + UV | Photo-oxidation system where a surrogate mixture is used to study the effects of individual compounds on overall SOA and ozone formation. |
| Surrogate + $NO_x$ + UV + $H_2O_2$ | Performed in parallel as control for surrogate containing experiments described immediately below. |
| IVOC + Surrogate + $NO_x$ + $H_2O_2$ + UV | Introduction of a test compound into the surrogate mixture can lead to competition for the hydroxyl radical. Experiments are conducted with 1 ppm $H_2O_2$ to reduce the impact of hydroxyl radical loss. |

**Table 3**
Chemical and physical properties of the select IVOCs tested.

| IVOC Compound[a] Name | CAS # | Chemical Formula | Molecular Structure | Boiling Point[b] °C | Vapor Pressure[a] mm Hg | $\overline{OS}c_0$[c] | $\log_{10}(C*)$ ug m$^{-3}$ |
|---|---|---|---|---|---|---|---|
| Propylene Glycol | 57-55-6 | $C_3H_8O_2$ | | 188 | 0.08 | −1.3 | 5.72 |
| Diethylene Glycol | 111-46-6 | $C_4H_{10}O_3$ | | 245 | 0.002 | −1.0 | 4.51 |
| Diethylene Glycol Ethyl Ether (DEGEE) | 111-90-0 | $C_6H_{14}O_3$ | | 202 | < 0.1 | −1.3 | 5.96 |
| Diethylene Glycol Monobutyl Ether (DEGBE) | 112-34-5 | $C_8H_{18}O_3$ | | 230 | 0.02 | −1.5 | 5.28 |
| Benzyl Alcohol | 100-51-6 | $C_7H_8O$ | | 205 | 0.094 @ 25 °C | −0.9 | 5.74 |
| Dipropylene Glycol Methyl Ether Acetate (DPGMEA) | 88917-22-0 | $C_9H_{18}O_4$ | | 209 | 0.08 | −1.1 | 5.91 |
| Dimethyl Glutarate (DBE-5) | 1119-40-0 | $C_7H_{12}O_4$ | | 215 | 0.097 | −0.6 | 4.33 |
| n-Tridecane (n-$C_{13}$) | 629-50-5 | $C_{13}H_{28}$ | | 234 | 0.08 @25 °C | −2.2 | 5.74 |
| n-Heptadecane (n-$C_{17}$) | 629-78-7 | $C_{17}H_{36}$ | | 302 | < 0.001 | −2.1 | 4.61 |
| 2,2,4-Trimethyl-1,3-Pentanediol Monoisobutyrate (Texanol®) | 25265-77-4 | $C_{12}H_{24}O_3$ | | 244 | 0.01 | −1.5 | 4.64 |
| Glyceryl Triacetate | 102-76-1 | $C_9H_{14}O_6$ | | 260 | 0.0025 @ 25 °C | −0.2 | 4.50 |
| Methyl Palmitate | 112-39-0 | $C_{17}H_{34}O_2$ | | 417 | 0.038 @ 25 °C | −1.8 | 2.90 |
| Triethanolamine | 102-71-6 | $C_6H_{15}NO_3$ | | 335 | 8.38e-6 @ 25 °C | −1.5 | 1.80 |
| Glycerol | 56-81-5 | $C_3H_8O_3$ | | 290 | 0.003 @50 °C | −0.7 | 1.83 |

[a] All the chemicals are purchased from Sigma-Aldrich (≥95.0–99.0%).
[b] Values are obtained from ACD/Labs Percepta Predictors—Software Modules.
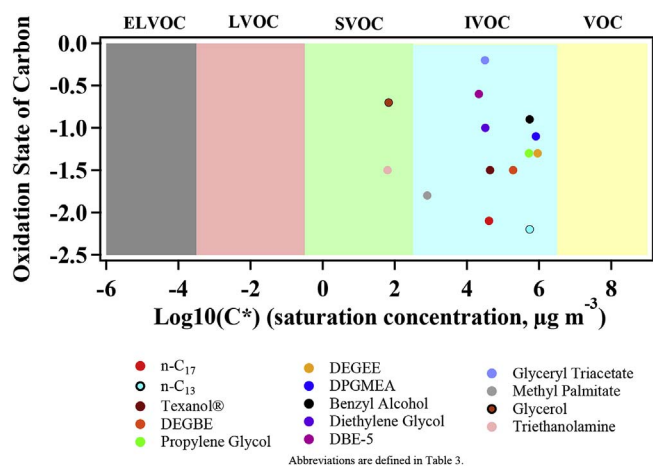[c] $\overline{OS}c_0$ is calculated based on the molecular structure of the IVOCs studied.



Fig. 2. Volatility and the extent of oxidation of the select IVOCs.

order of increasing volatility, gray shading refers to extremely low volatility organic compound (ELVOC, $C* < 3 \times 10^{-4}\,\mu g\,m^{-3}$), which stays almost entirely in the aerosol phase under ambient conditions. Light red shading stands for low volatility organic compound (LVOC, $3 \times 10^{-4} < C* < 0.3\,\mu g\,m^{-3}$). Light green shading represents semi-volatile organic compound (SVOC, $0.3 < C* < 300\,\mu g\,m^{-3}$). Light blue shading refers to intermediate volatility organic compound (IVOC, $300 < C* < 3 \times 10^6\,\mu g\,m^{-3}$). Yellow shading stands for volatile organic compound (VOC, $C* > 3 \times 10^6\,\mu g\,m^{-3}$). The C* values are obtained from Donahue et al., (2012). All of the individual compounds studied in this work are labelled on the figure with all compounds in the IVOC range except glycerol and Triethanolamine.

Evaporation rates of the IVOCs tested are evaluated gravimetrically with individual IVOC evaporation experiments commencing with 200 μl placed into a weighing boat. Benzyl alcohol, DEGBE, n-Tridecane, DBE-5, DPGMEA, DEGEE, and propylene glycol lose more than 95% of their mass within 1 month and Texanol® within 3 months (Abbreviations are defined in Table 3). Glyceryl triacetate, diethylene glycol, and n-Heptadecane lose half of their weight within 6 months. Glycerol, triethanolamine, and methyl palmitate lose less than 5% of their mass within six months.

Correlations of the IVOC evaporation rates to physical and chemical properties of the IVOCs are explored in an effort to provide semi-empirical prediction of the evaporation behavior for IVOCs studied. Previous studies show that evaporation rate from inert surfaces correlates well with vapor pressure (Woodrow et al., 1997, 2001; Guth et al., 2004). Later, Mackay and Wesenbeeck (2014) develop a simpler one parameter correlation for the evaporation rate of chemicals as a function of not only vapor pressure, but also molar mass. The relationship agrees with the assumption that the air immediately in contact with the liquid surface achieves a partial pressure of P (Pa). Therefore, the evaporation rate can be estimated as the product of the saturated vapor concentration and a mass-transfer coefficient. Their equation applies only to liquid surfaces that are not affected by the underlying solid substrate, such as selection of hydrocarbon carrier fluids used in emulsifiable concentrates in pesticide formulations and prediction of evaporation behavior of cleaning solvents applied to surfaces under fairly quiescent conditions.

In the current study, evaporation rate is calculated from the initial loss rate (initial slope) in Fig. 3 for each individual IVOC. Fig. 4 applies the correlation from Mackay and Wesenbeeck (2014)'s study and plots molar mass × vapor pressure versus evaporation rate with the constant designed in our systems for all IVOCs (Eqs. (1)). Experimental data exhibits a good linear trend ($R^2 = 0.98$), which indicates that the evaporation rates of IVOCs studied in this paper not only depend on their vapor pressures, but also correlate with their molar mass. This work extends the application of Mackay and Wesenbeeck's method
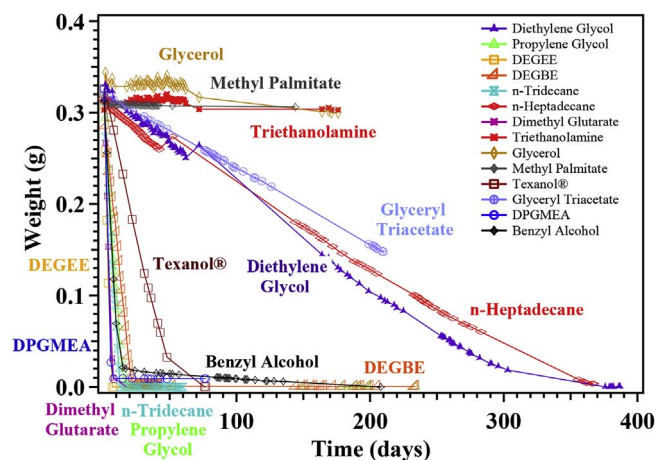
**Fig. 3.** Weight loss of the select IVOCs in evaporation chambers (Abbreviations are defined in Table 3).
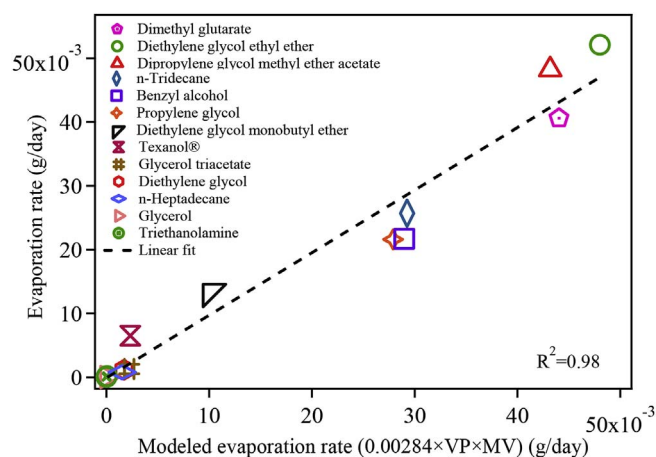


**Fig. 4.** Evaporation rate measured by the experiments and predicted by the evaporation model of the select IVOCs (calculated from weight loss results (Fig. 3).

(2014).

$$ER = 0.00284 \times VP \times MW \qquad (1)$$

where *ER* is the individual IVOC evaporation rate in g day$^{-1}$, *VP* is the vapor pressure in mmHg, and *MW* is the molar mass in g mol$^{-1}$.

### 3.2. SOA formation

As the extent of gas-particle partitioning is a function of organic aerosol concentration, the atmospheric representativeness of a given aerosol formation experiment is related to the final organic aerosol formed during a given experiment. Typically, ambient fine particle organic aerosol concentrations tend to be less than 10 µg m$^{-3}$. Rather than invest in obtaining full data sets necessary for yield curve determinations for just a few IVOCs, it is determined to measure SOA formation from a variety of IVOC precursors. Therefore, the SOA formation observed is used as a guidance as to the extent of SOA formation that might be expected from a variety of SOA precursors. The relative amounts of SOA formation from the IVOC precursors provide a strong indication of which IVOC precursors are important (or unimportant) SOA producers warranting further investigation. To calculate the mass concentration of the SOA, the SOA volumes established by SMPS measurements are wall-loss corrected following procedures detailed in Cocker et al. (2001) and then multiplied by measured SOA density.

### 3.2.1. Adding an IVOC to a surrogate ROG mixture

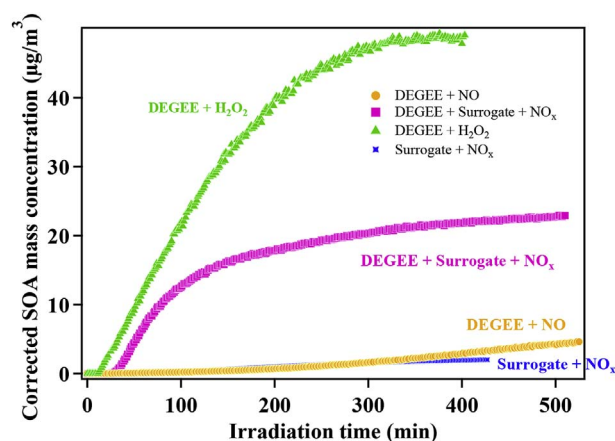As mentioned in the previous section, the surrogate consists of a



**Fig. 5.** Comparison of SOA formations from three different photo-oxidation systems.

simplified mixture designed to represent the major classes of hydrocarbons measured in ambient urban atmospheres, with one compound used to represent each class of model species used in condensed lumped-molecule mechanism (Carter et al., 2005). The surrogate is used as a tool to better simulate atmospheric reactivity during SOA and ozone formation in an urban environment. Fig. 5 shows SOA formation from photo-oxidation of DEGEE in the presence of NO only, H$_2$O$_2$ only, and both the surrogate mixture and NO$_x$. A surrogate/NO$_x$ experiment (no added IVOC) is also provided for comparison. Experimental conditions are summarized in Table 4. SOA formation is the highest for conditions that favor greater IVOC consumption, as illustrated in Fig. 5, where the higher OH radical concentration in the H$_2$O$_2$ only experiment is available to consume more DEGEE (Table 4). The second highest hydroxyl radical concentration is generated in the surrogate-NO$_x$-DEGEE experiment and therefore has the second greatest DEGEE consumption and SOA formation (Table 4). Without the presence of the surrogate mixture, the progression of the DEGEE-NO experiment to a point where NO consumption is complete is suppressed, thus delaying the evolution of excess peroxy and hydroperoxy radicals (Li et al., 2015). Therefore, it is not until the end of the DEGEE-NO experiment that conditions favoring SOA formation are achieved and measurable aerosol formation commenced in the relative absence of NO. NO depletion is achieved much earlier with surrogate mixture present. Further, due to the lower reactivity (hydroxyl radical generation) without the surrogate mixture, a smaller amount of DEGEE is consumed under NO only conditions. The surrogate-NO$_x$ run (no additional IVOC) does not form much SOA.

### 3.2.2. SOA formation from select individual IVOCs

Fig. 6 presents the SOA formation from individual IVOCs when oxidized in the presence of the surrogate, NO$_x$ and UV. SOA mass concentration is normalized by total mass of precursor consumed. One might expect that the selected IVOCs with lower vapor pressures than traditionally studied VOCs would have greater propensity to form SOA. However, these findings demonstrate that half of the select IVOCs did not form appreciable SOA. Benzyl Alcohol, n-Heptadecane, and DEGBE have the most significant aerosol formation, while DEGEE, n-Tridecane, and DBE-5 show moderate aerosol formation. The largest rate of SOA formation occurred within the first two hours of photo-oxidation, coinciding with highest OH concentrations, estimated from the decay of *m*-xylene. The higher the SOA formation is, the faster the formation rate of SOA is during the first two hours of photo-oxidation. The SOA formation from n-Tridecane and DBE-5 are delayed, which may have been due to formation of low-volatility compounds through multi-generation processes.

A series of experiments are conducted with enhanced OH reactivity by injecting 1.0 ppm H$_2$O$_2$, which allows for greater consumption of the

**Table 4**
Experimental conditions for runs listed in Fig. 5.

| Experimental conditions | Surrogate$_0$[a] (ppmC) | NO[b] (ppb) | NO$_2$[b] (ppb) | DEGEE$_0$[c] (ppb) | OH (molec cm$^{-3}$) | ΔDEGEE[d] (μg m$^{-3}$) | ΔM[e] (μg m$^{-3}$) | Yield |
|---|---|---|---|---|---|---|---|---|
| Surrogate + NO$_x$ | 1.1 | ~16 | ~9 | – | 1.52E+08 | – | 2.3 | – |
| DEGEE + NO | – | ~20 | – | 40 | 6.49E+07 | 168.0 | 4.6 | 0.03 |
| Surrogate + NO$_x$ + DEGEE | 1.1 | ~16 | ~9 | 40 | 9.96E+07 | 338.2 | 23.0 | 0.07 |
| DEGEE + H$_2$O$_2$ | – | – | – | 40 | 3.66E+8 | 360.9 | 49.1 | 0.2 |

[a] Initial surrogate ROG mixture concentration.
[b] Initial NO and NO$_2$ concentration.
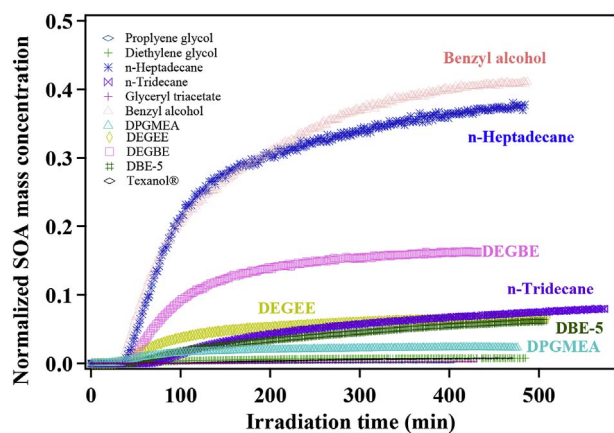[c] Initial DEGEE concentration.
[d] DEGEE reacted.
[e] SOA formed.



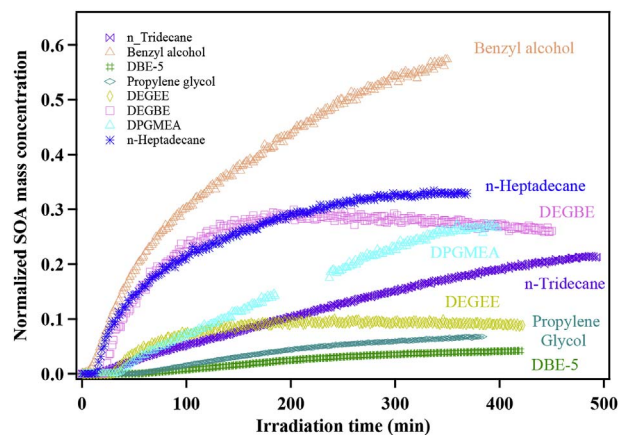**Fig. 6.** Normalized SOA formation by total precursor consumed from select individual IVOCs with surrogate and NO$_x$.



**Fig. 8.** Comparison of SOA formation with and without H$_2$O$_2$ for select IVOCs in the presence of NO$_x$ and surrogate.



**Fig. 7.** Normalized SOA formation by total precursor consumed from individual IVOCs with surrogate, NO$_x$, and H$_2$O$_2$.

initial IVOC by offsetting losses in reactivity due to hydroxyl radical consumption. Fig. 7 illustrates the normalized SOA formation from individual IVOCs with surrogate, NO$_x$, UV, and H$_2$O$_2$. Benzyl Alcohol, n-Heptadecane, DPGMEA, DEGBE, and n-Tridecane all show significant aerosol formation. DEGEE, Propylene Glycol, and DBE-5 show moderate aerosol formation. The SOA formed from DEGEE and DEGBE is observed to decrease slightly during the last 3 h of the experiments, which may indicate that some semi-volatile species partition back from aerosol phase to gas phase and fragmented during further oxidation (Li and Cocker, 2017). The SOA formations from n-Tridecane, DPGMEA, DBE-5, Propylene Glycol, DEGEE and DEGBE are all delayed, which may be due to formation of low-volatility compounds through multi-generation processes.

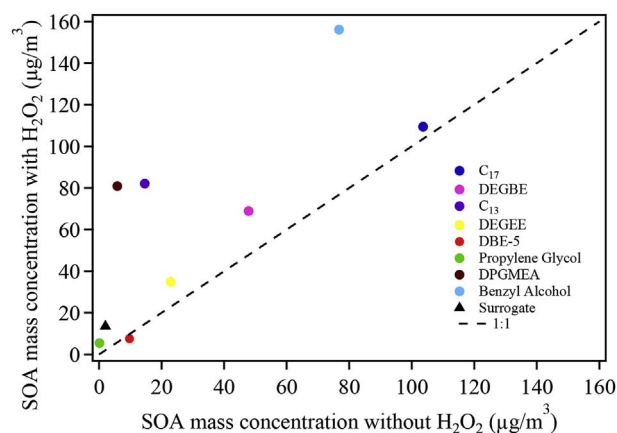Fig. 8 confirms that more SOA formation occurs for IVOCs in the presence H$_2$O$_2$ than without. DPGMEA does not form observable SOA without H$_2$O$_2$ addition, but forms appreciable amount of SOA in the presence of H$_2$O$_2$. Adding H$_2$O$_2$ creates twice and five times the SOA formation from Benzyl Alcohol and n-Tridecane, respectively. Adding H$_2$O$_2$ does not significantly affect SOA formation from n-Heptadecane indicating that the SOA formation is dominated by sufficiently first generation low volatility products which do not react further to form appreciable additional SOA. The other reason could be that some semi-volatile products partition back to gas phase through continuous oxidation.

### 3.2.3. SOA mass yields of select individual IVOCs

To compare the SOA formation across individual IVOCs, an effective SOA mass yield is calculated for each IVOC using an approach similar to that of Odum et al. (1996, 1997a, 1997b). The definition of the effective SOA mass yield ($Y$) used in this study is the ratio of the particle wall-loss-corrected SOA mass ($\Delta M_0$) to the estimated mass of IVOC reacted ($\Delta HC$) (Eq. (2)).

$$Y = \frac{\Delta M_0}{\Delta HC} \qquad (2)$$

The amount of IVOC reacted is calculated by assuming that each IVOC undergoes a first order reaction with the OH radical (Eq. (3)),

$$\frac{d[C_i]}{dt} = -k_{OH,C_i}[OH][C_i] \qquad (3)$$

where $[C_i]$ is the individual IVOC concentration in μg m$^{-3}$, $k_{OH}$ is the reaction rate constant in cm$^3$ (molecules·s)$^{-1}$, [OH] is the OH radical concentration in molecules cm$^{-3}$. The reaction rate constants ($k_{OH}$) for each IVOC are taken from the literature and are listed in Table S3. [OH] is estimated using decay of m-xylene. Excellent consistency is seen between yields obtained from calculated and measured IVOC decay for IVOCs with available concentration data (Fig. S1). SOA yields from photo-oxidation of IVOCs with surrogate and NO$_x$ range from < 0%
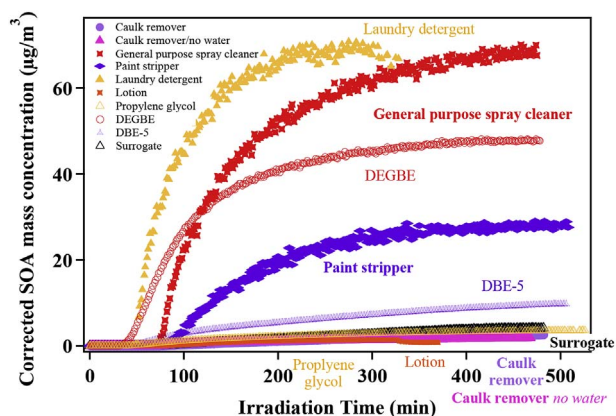
**Fig. 9.** Comparison of SOA formation from single IVOCs with that from mixtures in the presence of surrogate and $NO_x$.



**Fig. 10.** SOA formation from IVOCs containing generic consumer products with surrogate, $NO_x$, and $H_2O_2$.

(negligible) to 41% (Table S4). SOA yields from photo-oxidation of select IVOCs with surrogate, $NO_x$, and $H_2O_2$ range from < 1% (negligible) to 56% (Table S4). Individual aerosol yield experiments are insufficient to fit empirical two-product models or Volatility Basis Sets (VBS) (Donahue et al., 2012). However, the values obtained still provide insight into those IVOCs that are most likely to form SOA. While the initial hypothesis is that IVOCs would form significant SOA, only Benzyl Alcohol, n-Heptadecane, and DEGBE have yields greater than 0.1 (without additional $H_2O_2$). Addition of $H_2O_2$ adds DEGBE, and DPGMEA to the list of SOA precursors with yields > 0.1.

### 3.2.4. SOA formation from select IVOC-containing consumer products

Fig. 9 plots the SOA formation from several consumer products in the presence of surrogate and $NO_x$. SOA formation from corresponding individual IVOCs present in the consumer product is shown as comparison. The IVOC in consumer product quantity matches to the individual IVOC experiment except for laundry detergent and lotion runs, where the Propylene Glycol quantity are 2 times higher than that in individual Propylene Glycol experiments. For the caulk remover without water run, the top three major components (dimethyl glutarate, dimethyl succinate, and dimethyl adipate) in the caulk remover mixture are injected instead of adding the whole mixture. The amount of the three IVOCs injected matches the amount of the three IVOCs present in the caulk remover with water run. Fig. 9 illustrates that laundry detergent, general purpose spray cleaner, and paint stripper (from most to least) each forms appreciable amounts of SOA compared to that formed from the surrogate ROG mixture alone while the hand lotion and caulk remover (with or without water) form only minimal amounts of SOA compared to that formed from the surrogate only experiment. General purpose spray cleaner contains DEGBE and more aerosols are formed in the general spray cleaner mixture than by that from DEGBE alone. Similarly, the laundry detergent mixture forms more aerosol than its IVOC, propylene glycol. Both paint stripper and caulk remover contain DBE-5. However, DBE-5 aerosol behave differently in the two different product mixtures. Paint stripper forms more aerosol than DBE-5 while caulk remover forms less aerosol than DBE-5.

Clearly, the presence of other chemicals in the consumer product influences the reactivity and aerosol formation routes. For instance, the paint stripper contains 5% d-limonene, a known reactive compound individually capable of forming significant amounts of SOA (and ozone) (Kundu et al., 2012), which is expected to have an additive effect on the SOA formed from the individual IVOC. The additive effect includes both increased reactivity of the IVOC (More is consumed) as well as the additional SOA produced by the d-limonene itself. This further leads to greater SOA formation as more SOA present increases the expected SOA yield of the compound through increased sorptive partitioning. Conversely, other ingredients in the caulk remover may be acting as a
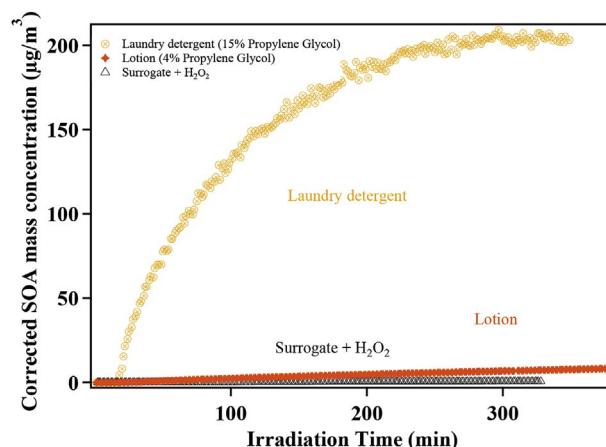
hydroxyl radical scavenger reducing the extent of IVOC oxidation and thus SOA formation from the caulk remover compared to the individual compound itself.

Two consumer products (laundry detergent and lotion) are studied in the presence of the surrogate mixture with enhanced $H_2O_2$ (Fig. 10). The hand lotion still produces little SOA while the SOA formation from laundry detergent is greatly enhanced. The SOA enhancement for laundry detergent is consistent with enhancements seen for individual IVOCs (however, SOA formation is much greater than that anticipated from Propylene Glycol). The hand lotion is difficult to inject, which may have led to lower SOA formation than expected from the mixture.

### 3.2.5. Trends in SOA elemental composition and SOA physical properties

Table S1 summarizes the oxygen-to-carbon (O:C) and hydrogen-to-carbon (H:C) ratios along with other physical properties of SOA, including density and volatile fraction remaining (VFR) for all the experiments. VFR ($VFR = d^3/d_0^3$, d (particle final mobility diameter) and $d_0$ (particle initial mobility diameter)) is used to describe bulk SOA volatility after heating SOA at a fixed temperature (17 °C) in a thermodenuder for a short period of time (17s). Fig. 11 plots ΔO:C against SOA mass concentration. The ΔO:C is calculated by subtracting the initial O:C of SOA forming precursor from the final O:C, which is an averaged value over the last one hour. A general increase of the ΔO:C ratio as the SOA mass concentration increases is observed, suggesting that the amount of SOA formed is dependent on SOA chemical
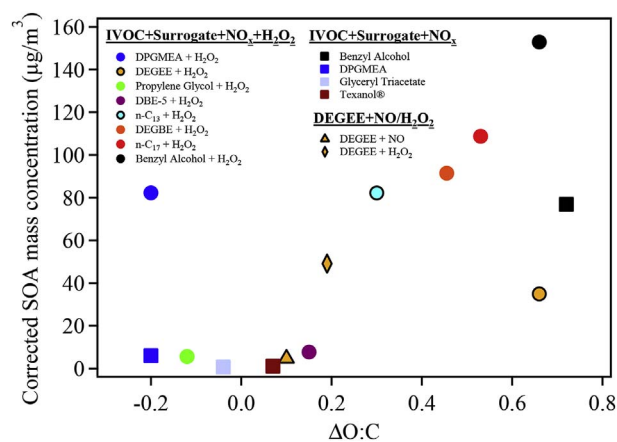


**Fig. 11.** Correlation between the change of oxygen to carbon ratio (ΔO:C) and SOA mass concentration for all the runs producing > 2 μg m⁻³ of aerosol with available AMS data. Data collected under different experimental conditions are identified by different markers.
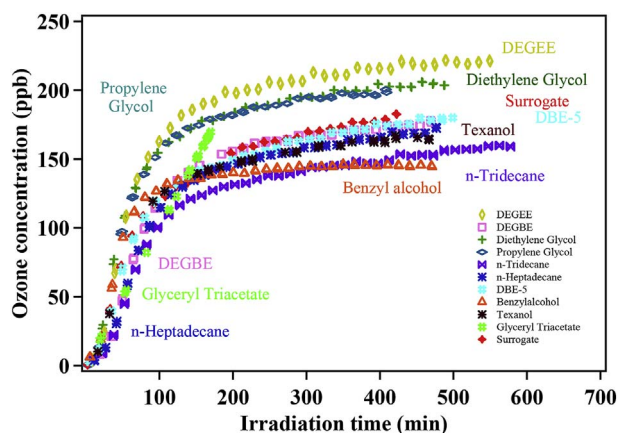
**Fig. 12.** Ozone formation from individual IVOCs with surrogate and $NO_x$.

composition. Several experiments, most notably DPGMEA, are observed to have ΔO:C less than zero, attributable to loss of oxygen during fragmentation processes or through dehydration reactions. Fig. S2 and Fig. S3 explore the relationship among $\overline{OSc}$, volatility, and SOA yield for photo-oxidation of select IVOCs. Fig. S4 shows the relationship between VFR and $\overline{OSc}$.

### 3.3. Ozone formation from select individual IVOCs

Fig. 12 presents the results of ozone formation from individual IVOCs with surrogate and $NO_x$. The final ozone concentrations range from 145 to 222 ppb. DEGEE, Diethylene Glycol, Glycerol Triacetate, and Propylene Glycol show enhanced $O_3$ formation, while DBE-5 and DEGBE are similar to the surrogate only $O_3$ formation, and the presence of n-Tridecane, n-Heptadecane, Benzyl Alcohol, and Texanol® reduces the $O_3$ formed from the surrogate mixture.

It is important to note that a decrease in ozone formed with the addition of the IVOC does not necessarily indicate that the IVOC will suppress ozone formation in the atmosphere—only that it is negatively impacting the specific surrogate mixture ozone formation. This may be attributed to larger changes in radical concentrations, $NO_x$ loadings, etc. than expected to occur within the more complex ambient atmosphere with its more significant reservoir. This has been observed and discussed previously (Carter, 2011). For example, in the n-Tridecane and n-Heptadecane case, heavy alkanes could be radical inhibitors, which will prevent cycling OH radicals back by generating $RONO_2$ instead of RO· (Carter, 2011). Therefore, addition of n-Tridecane and n-Heptadecane reduces the overall hydroxyl concentrations available to oxidize both the IVOC and the ozone forming surrogate hydrocarbons relative to the amount of oxidation and ozone that forms in the surrogate photo-oxidation alone. If the reduction is large enough and the experiment is sensitive enough to this reduction in hydroxyl radical then less net $O_3$ formation will occur when the added IVOC is present. The sensitivity of the experiment to reduced radical levels depends on the conditions of the experiment, and calculations indicate that most of our experiments are more sensitive to reduced radical levels than is the case for atmospheric conditions where the relative abundance of the IVOC to other VOCs participating in the reaction is lower (Carter, 2011).

As to the Benzyl alcohol and Texanol® case, the ozone formation rate is faster than that of the surrogate but also plateaus at a lower ozone concentration. The probable explanation is that under low $NO_x$ conditions, the availability of $NO_x$ throughout the experiment determines how much ozone will ultimately form. Although the ozone forms faster under this condition, if there is a VOC or IVOC that removes $NO_x$ at a faster rate and the experiment is sensitive enough to $NO_x$ conditions, there will be less $NO_x$ available to form ozone. Once the $NO_x$ is consumed, ozone will stop forming. The experiments measure the effects of

the test compounds or mixtures on ozone formation under the chamber environment. Because of different sensitivities to effects on radical levels and other factors, the effects on ozone in the chamber is not exactly the same as their effects on ozone in the atmosphere.

An additional series of experiments with enhanced hydroxyl radical concentration is performed to exercise the performance of the model and offset losses in hydroxyl reactivity in the mixture due to the addition of the IVOC (Fig. S5). Direct comparisons of ozone formation for select IVOCs with and without $H_2O_2$ are shown in Fig. S6. Ozone formation rate is faster when adding $H_2O_2$. Fig. S7 and Fig. S8 illustrate ozone formation from select IVOCs-containing consumer products in the presence and absence of $H_2O_2$. Ozone Modeling Results from the SAPRC-11 Mechanism is shown in Fig. S9. Generally, acceptable agreement is observed between the IVOC experiments within this work and that predicted by the current SAPRC-11 model, with the model giving good simulations (Fig. S9), and simulating the impacts of the added compounds within the range observed previously for similar compounds (Carter, 2010).

### 4. Conclusion

The evaporation rates of 14 IVOCs that are also classified as LVP-VOCs are measured. Half of these IVOCs lose more than 95% of their mass within a month suggesting that these compounds, which are exempted from VOC regulations as LVP-VOCs, may be evaporate under ambient conditions for SOA and ozone formation. SOA formations from the individual IVOCs studied vary widely with nearly half of the IVOCs explored not forming measurable SOA while other IVOCs producing appreciable SOA. Further detailed studies are required to determine functional relationships of other IVOC compound types to improve forecasting of ability of other types of IVOCs to form SOA. Ozone formations from several individual IVOCs are suppressed, which indicates that the IVOCs act as either radical inhibitors or removed $NO_x$ at a faster rate than the surrogate mixture. The current SAPRC-11 model predicts ozone formation from select IVOCs well, and the current maximum incremental reactivity (MIR) values associated with the compounds are expected to be good. The addition of lab created generic consumer products (general purpose spray cleaner, paint stripper, caulk remover, laundry detergent, and hand lotion) has a weak influence on ozone formation from the surrogate mixture but strongly affects SOA formation. Other components, beyond the individually identified IVOCs also strongly contribute to aerosol formation as the total aerosol formation observed could not be explained solely by the individual aerosol forming IVOCs studied. The overall SOA and ozone formation of the generic consumer product could not be explained solely by analyzing the results of the pure IVOC experiments.

### Appendix A. Supplementary data

Supplementary data related to this article can be found at http://dx.doi.org/10.1016/j.atmosenv.2017.12.019.

### References

Bernard, F., Magneron, I., Eyglunent, G., Daële, V., Wallington, T.J., Hurley, M.D., Mellouki, A., 2013. Atmospheric chemistry of benzyl alcohol: kinetics and mechanism of reaction with OH radicals. Environ. Sci. Technol. 47, 3182–3189.
California Air Resources Board (CARB), 2015. Regulation for Reducing Emissions from

Consumer Products. Title 17, California Code of Regulations, Division 3, (Chapter 1), Sub(chapter 8).5, Article 2 pp. 94507–94517. Available online at: https://www.arb.ca.gov/consprod/regs/regs.htm.

Cappa, C.D., Jathar, S.H., Kleeman, M.J., Docherty, K.S., Jimenez, J.L., Seinfeld, J.H., Wexler, A.S., 2016. Simulating secondary organic aerosol in a regional air quality model using the statistical oxidation model – Part 2: assessing the influence of vapor wall losses. Atmos. Chem. Phys. 16, 3041–3059.

Carter, W.P.L., Luo, D., Malkina, I.L., Pierce, J.A., 1995. Environmental Chamber Studies of Atmospheric Compounds. Effects of Varying ROG Surrogate and NOₓ. Final Report to California Air Resources Board, Contract A032–096, Coordinating Research Council, Inc., Project ME-9, National Renewable Energy Laboratory, Contract ZF-2-12252, South Coast Air Quality Management District, Contract C91323.

Carter, W.P.L., Cocker III, D.R., Fitz, D.R., Malkina, I.L., Bumiller, K., Sauer, C.G., Pisano, J.T., Bufalino, C., Song, C., 2005. A new environmental chamber for evaluation of gas- phase chemical mechanisms and secondary aerosol formation. Atmos. Environ. 39 (40), 7768–7788.

Carter, W.P.L., 2010. Development of the SAPRC-07 chemical mechanism. Atmos. Environ. 44, 5324–5335.

Carter, W.P.L., 2011. Environmental Chamber Study of Ozone Impacts of Coatings VOCs. Final report to California Air Resources Board, Contract No. 07–339, May 11 Available at: http://www.cert.ucr.edu/ ~ carter/absts.htm#coatrpt2.

Carter, W.P.L., Heo, G., Cocker III, D.R., Nakao, S., 2012. SOA Formation: Chamber Study and Model Development. Final Report to the California Air Resources Board Contract No. 08–326.

Chan, A.W.H., Kautzman, K.E., Chhabra, P.S., Surratt, J.D., Chan, M.N., Crounse, J.D., Kurten, A., Wennberg, P.O., Flagan, R.C., Seinfeld, J.H., 2009. Secondary organic aerosol formation from photooxidation of naphthalene and alkylnaphthalenes: implications for oxidation of intermediate volatility organic compounds (IVOCs). Atmos. Chem. Phys. 9 (9), 3049–3060.

Chen, C., Kacarab, M., Tang, P., Cocker III, D.R., 2016. SOA formation from naphthalene, 1-methylnaphthalene, and 2-methylnaphthalene photooxidation. Atmos. Environ. 131, 424–433.

Cocker III, D.R., Flagan, R.C., Seinfeld, J.H., 2001. State-of-the-art chamber facility for studying atmospheric aerosol chemistry. Environ. Sci. Technol. 35 (12), 2594–2601.

Cocker III, D.R., Li, L., Price, D., Kacarab, M., Chen, C., 2014. Review of VOC Emissions Inventory for Consumer Products and Architectural Coatings for Potential Alternative Fate and Availability Corrections. Consumer Specialty Products Association.

DeCarlo, P.F., Kimmel, J.R., Trimborn, A., Northway, M.J., Jayne, J.T., Aiken, A.C., Gonin, M., Fuhrer, K., Horvath, T., Docherty, K.S., Worsnop, D.R., Jimenez, J.L., 2006. Field-deployable, high-resolution, time-of-flight aerosol mass spectrometer. Anal. Chem. 78 (24), 8281–8289.

Donahue, N.M., Kroll, J.H., Pandis, S.N., Robinson, A.L., 2012. A two-dimensional volatility basis set – Part 2: diagnostics of organic-aerosol evolution. Atmos. Chem. Phys. 12, 615–634.

Finlayson-Pitts, B.J., Pitts Jr., J.N., 1993. Atmospheric chemistry of tropospheric ozone formation: scientific and regulatory implications. Air Waste 43, 1091–1100.

Gentner, D.R., Isaacman, G., Worton, D.R., Chan, A.W.H., Dallmann, T.R., Davis, L., Liu, S., Day, D.A., Russell, L.M., Wilson, K.R., Weber, R., Guha, A., Harley, R.A., Goldstein, A.H., 2012. Elucidating secondary organic aerosol from diesel and gasoline vehicles through detailed characterization of organic carbon emissions. Proc. Natl. Acad. Sci. Unit. States Am. 109 (45), 18318–18323.

Guth, J.A., Reischmann, F.J., Allen, R., Arnold, D., Hassink, J., Leake, C.R., Skidmore, M.W., Reeves, G.L., 2004. Volatilisation of crop protection chemicals from crop and soil surfaces under controlled conditions-prediction of volatile losses from physico-chemical properties. Chemosphere 57, 871–887.

Hallquist, M., Wenger, J.C., Baltensperger, U., Rudich, Y., Simpson, D., Claeys, M., Dommen, J., Donahue, N.M., George, C., Goldstein, A.H., Hamilton, J.F., Herrmann, H., Hoffmann, T., Iinuma, Y., Jang, M., Jenkin, M.E., Jimenez, J.L., Kiendler-Scharr, A., Maenhaut, W., McFiggans, G., Mentel, T.F., Monod, A., Prevot, A.S.H., Seinfeld, J.H., Surratt, J.D., Szmigielski, R., Wildt, J., 2009. The formation, properties and impact of secondary organic aerosol: current and emerging issues. Atmos. Chem. Phys. 9, 5155–5236.

Jathar, S.H., Woody, M., Pye, H.O.T., Baker, Kirk R., Robinson, A.L., 2017. Chemical transport model simulations of organic aerosol in southern California: model evaluation and gasoline and diesel source contributions. Atmos. Chem. Phys. 17, 4305–4318.

Krechmer, J.E., Pagonis, D., Ziemann, P.J., Jimenez, J.L., 2016. Quantification of gas-wall partitioning in Teflon environmental chambers using rapid bursts of low-volatility oxidized species generated in situ. Environ. Sci. Technol. 50, 5757–5765.

Kroll, J.H., Donahue, N.M., Jimenez, J.L., Kessler, S.H., Canagaratna, M.R., Wilson, K.R., Altieri, K.E., Mazzoleni, L.R., Wozniak, A.S., Bluhm, H., Mysak, E.R., Smith, J.D., Kolb, C.E., Worsnop, D.R., 2011. Carbon oxidation state as a metric for describing the chemistry of atmospheric organic aerosol. Nat. Chem. 3, 133–139.

Kundu, S., Fisseha, R., Putman, A.L., Rahn, T.A., Mazzoleni, L.R., 2012. High molecular weight SOA formation during limonene ozonolysis: insights from ultrahigh-resolution FT-ICR mass spectrometry characterization. Atmos. Chem. Phys. 12, 5523–5536.

Li, L., Cocker III, D.R., 2017. Molecular structure impacts on secondary organic aerosol formation from glycol ethers. Atmos. Environ.

Li, L., Tang, P., Cocker, D.R., 2015. Instantaneous nitric oxide effect on secondary organic aerosol formation from m-xylene photooxidation. Atmos. Environ. 119, 144–155. http://dx.doi.org/10.1016/j.atmosenv.2015.08.010.

Lim, Y.B., Ziemann, P.J., 2005. Products and mechanism of secondary organic aerosol formation from reactions of n-alkanes with OH radicals in the presence of NOₓ.

Environ. Sci. Technol. 39 (23), 9229–9236.

Lim, Y.B., Ziemann, P.J., 2009. Chemistry of secondary organic aerosol formation from OH radical-initiated reactions of linear, branched, and cyclic alkanes in the presence of NOₓ. Aero. Sci. Technol. 43, 604–619.

Loza, C.L., Craven, J.S., Yee, L.D., Coggon, M.M., Schwantes, R.H., Shiraiwa, M., Zhang, X., Schilling, K.A., Ng, N.L., Canagaratna, M.R., Ziemann, P.J., Flagan, R.C., Seinfeld, J.H., 2014. Secondary organic aerosol yields of 12-carbon alkanes. Atmos. Chem. Phys. Discuss. 13, 20677–20727.

Ma, P.K., Zhao, Y., Robinson, A.L., Worton, D.R., Goldstein, A.H., Ortega, A.M., Jimenez, J.L., Zotter, P., Prévôt, A.S.H., Szidat, S., Hayes, P.L., 2017. Evaluating the impact of new observational constraints on P-S/IVOC emissions, multi-generation oxidation, and chamber wall losses on SOA modeling for Los Angeles, CA. Atmos. Chem. Phys. 17, 9237–9259.

Mackay, D., Wesenbeeck, I.V., 2014. Correlation of chemical evaporation rate with vapor pressure. Environ. Sci. Technol. 48, 10259–10263.

Malloy, Q., Nakao, S., Switzer, D., Cocker, D., Hagino, H., 2009. On-line density measurements of secondary organic aerosol formation. Aero. Sci. Technol. 43, 673–678.

Matsunaga, A., Ziemann, P.J., 2010. Gas-wall partitioning of organic compounds in a Teflon film chamber and potential effects on reaction product and aerosol yield measurements. Aero. Sci. Technol. 44 (10), 881–892.

Naeher, L.P., Brauer, M., Lipsett, M., Zelikoff, J.T., Simpson, C.D., Koenig, J.Q., Smith, K.R., 2007. Woodsmoke health effects: a review. Inhal. Toxicol. 19, 67–106.

Odum, J.R., Hoffmann, T., Bowman, F., Collins, D., Flagan, R.C., Seinfeld, J.H., 1996. Gas/particle partitioning and secondary organic aerosol yields. Environ. Sci. Technol. 30, 2580–2585.

Odum, J.R., Jungkamp, T.P.W., Griffin, R.J., Flagan, R.C., Seinfeld, J.H., 1997a. The atmospheric aerosol-forming potential of whole gasoline vapor. Science 276, 96–99.

Odum, J.R., Jungkamp, T.P.W., Griffin, R.J., Forstner, H.J.L., Flagan, R.C., Seinfeld, J.H., 1997b. Aromatics, reformulated gasoline, and atmospheric organic aerosol formation. Environ. Sci. Technol. 31, 1890–1897.

Presto, A.A., Miracolo, M.A., Kroll, J.H., Worsnop, D.R., Robinson, A.L., Donahue, N.M., 2009. Intermediate-volatility organic compounds: a potential source of ambient oxidized organic aerosol. Environ. Sci. Technol. 43, 4744–4749.

Presto, A.A., Miracolo, M.A., Donahue, N.M., Robinson, A.L., 2010. Secondary organic aerosol formation from high-NOₓ photo-oxidation of low volatility precursors: n-alkanes. Environ. Sci. Technol. 44, 2029–2034.

Qin, T.F.D., Plattner, G.-K., Tignor, M., Allen, S.K., Boschung, J., Nauels, A., Xia, Y., Bex, V., Midgley, P.M., 2013. Climate Change 2013: the Physical Science Basis. Contribution of Working Group I to the Fifth Assessment Report of the Intergovernmental Panel on Climate Change. Cambridge University Press, pp. 1535.

Rader, D.J., McMurry, P.H., 1986. Application of the tandem differential mobility analyzer to studies of droplet growth or evaporation. J. Aerosol Sci. 17 (5), 771–787.

Robinson, A.L., Donahue, N.M., Shrivastava, M.K., Weitkamp, E.A., Sage, A.M., Grieshop, A.P., Lane, T.E., Pierce, J.R., Pandis, S.N., 2007. Rethinking organic aerosols: semi-volatile emissions and photochemical aging. Science 315, 1259–1262.

Sage, A.M., Weitkamp, E.A., Robinson, A.L., Donahue, N.M., 2008. Evolving mass spectra of the oxidized component of organic aerosol: results from aerosol mass spectrometer analyses of aged diesel emissions. Atmos. Chem. Phys. 8, 1139–1152.

Shin, H.-M., McKone, T.E., Bennett, D.H., 2016. Volatilization of low vapor pressure – volatile organic compounds (LVP-VOCs) during three cleaning products-associated activities: potential contributions to ozone formation. Chemosphere 153, 130–137.

Tkacik, D.S., Presto, A.A., Donahue, N.M., Robinson, A.M., 2012. Secondary organic aerosol formation from intermediate-volatility organic compounds: cyclic, linear, and branched alkanes. Environ. Sci. Technol. 46, 8773–8781.

Vo, U.-U.T., Morris, M.P., 2014. Nonvolatile, semivolatile, or volatile: redefining volatile for volatile organic compounds. J. Air Waste Manag. Assoc. 64, 661–669.

Weitkamp, E.A., Sage, A.M., Pierce, J.R., Donahue, N.M., Robinson, A.L., 2007. Organic aerosol formation from photochemical oxidation of diesel exhaust in a smog chamber. Environ. Sci. Technol. 41, 6969.

Woodrow, J.E., Seiber, J.N., Baker, L.W., 1997. Correlation techniques for estimating pesticide volatilization flux and downwind concentrations. Environ. Sci. Technol. 31, 523–529.

Woodrow, J.E., Seiber, J.N., Dary, C., 2001. Predicting pesticide emissions and downwind concentrations using correlations with estimated vapor pressures. J. Agric. Food Chem. 49, 3841–3846.

Ye, P., Ding, X., Hakala, J., Hofbauer, V., Robinson, E.S., Donahue, N.M., 2016. Vapor wall loss of semi-volatile organic compounds in a Teflon chamber. Aero. Sci. Technol. 50 (8), 822–834.

Yee, L.D., Kautzman, K.E., Loza, C.L., Schilling, K.A., Coggon, M.M., Chhabra, P.S., Chan, M.N., Chan, A.W.H., Hersey, S.P., Crounse, J.D., Wennberg, P.O., Flagan, R.C., Seinfeld, J.H., 2013. Secondary organic aerosol formation from biomass burning intermediates: phenol and methoxyphenols. Atmos. Chem. Phys. Discuss. 13, 3485–3532.

Yeh, G.K., Ziemann, P.J., 2014. Alkyl nitrate formation from the reactions of C₈–C₁₄ n-alkanes with OH radicals in the presence of NOₓ: measured yields with essential corrections for gas–wall partitioning. J. Phys. Chem. A 118, 8147–8157.

Zhang, X., Cappa, C.D., Jathar, S.H., McVay, R.C., Ensberg, J.J., Kleeman, M.J., Seinfeld, J.H., 2014. Influence of vapor wall loss in laboratory chambers on yields of secondary organic aerosol. Proc. Natl. Acad. Sci. Unit. States Am. 111 (16), 5802–5807.

Zhao, Y.L., Hennigan, C.J., May, A.A., Tkacik, D.S., de Gouw, J.A., Gilman, J.B., Kuster, W.C., Borbon, A., Robinson, A.L., 2014. Intermediate-volatility organic compounds: a large source of secondary organic aerosol. Environ. Sci. Technol. 48, 13743–13750.